

## Realization of a Fermi-Hubbard Optical Tweezer Array

Benjamin M. Spar<sup>1</sup>, Elmer Guardado-Sanchez<sup>1,\*</sup>, Sungjae Chi<sup>1</sup>, Zoe Z. Yan<sup>1</sup>, and Waseem S. Bakr<sup>1,†</sup>

*Department of Physics, Princeton University, Princeton, New Jersey 08544, USA*

 (Received 28 October 2021; accepted 18 April 2022; published 1 June 2022)

We use lithium-6 atoms in an optical tweezer array to realize an eight-site Fermi-Hubbard chain near half filling. We achieve single site detection by combining the tweezer array with a quantum gas microscope. By reducing disorder in the energy offsets to less than the tunneling energy, we observe Mott insulators with strong antiferromagnetic correlations. The measured spin correlations allow us to put an upper bound on the entropy of  $0.26(4)k_B$  per atom, comparable to the lowest entropies achieved with optical lattices. Additionally, we establish the flexibility of the tweezer platform by initializing atoms on one tweezer and observing tunneling dynamics across the array for uniform and staggered 1D geometries.

DOI: [10.1103/PhysRevLett.128.223202](https://doi.org/10.1103/PhysRevLett.128.223202)

Arrays of neutral atoms in optical tweezers have emerged as a powerful new platform for quantum simulation and computation [1–3]. It is now possible to study interacting quantum systems in defect-free tweezer arrays with hundreds of atoms [4,5]. Initial work with reconfigurable tweezer arrays used alkali atoms, and the platform has now expanded to include alkaline earth atoms [6–8] and molecules [9,10]. Notable results include studies of quantum spin models using atoms excited to Rydberg states [11,12], demonstration of high fidelity quantum gates [13,14], and high quality factor atomic clocks [15]. Most of the activity with tweezer arrays has focused on atoms localized on individual tweezers. The versatility of tweezer arrays provides a strong incentive for extending quantum simulations with this platform to systems of mobile atoms where the effects of quantum statistics become important. A key step in this direction has been the demonstration of tunnel-coupled double-well tweezer systems [16,17].

The use of tweezer arrays to study itinerant condensed matter models such as the Hubbard model realizes a “bottom-up” paradigm of quantum simulation, in contrast to the more established “top-down” approach of using optical lattices [18]. Optical lattices are an efficient way to create periodic trapping potentials with thousands of lattice sites that can be loaded directly from a degenerate gas. In recent years, quantum gas microscopes have been used to probe optical lattices with single-site resolution, allowing for extraction of multipoint correlation functions. In particular, fermionic quantum gas microscopes have been used to explore the phase diagram of the square lattice Fermi-Hubbard model, a minimal model for high temperature superconductivity [19]. Quantum gas microscopes have allowed for direct measurement of the Mott insulator state [20,21], antiferromagnetic correlations at half filling [22–25], and the motion of a single hole in an antiferromagnetic background [26–28].

Studying Fermi-Hubbard models with optical lattices faces two challenges that motivate the consideration of tweezer arrays as an alternative platform. First, the lowest entropies that have been achieved for correlated states in optical lattices are in the range of  $0.3\text{--}0.5k_B$  per particle [29–31]. This has hindered access to interesting regimes of the square Hubbard model phase diagram such as the pseudogap or the putative  $d$ -wave superconductor [32]. Sophisticated entropy redistribution schemes have been investigated, but were limited by the ability to precisely control lattice potentials at the single-site level [33]. A second challenge, particularly relevant for microscope experiments, is the difficulty of reconfiguring the apparatus to study different lattice geometries. Programmable Fermi-Hubbard tweezer arrays have the potential to address both of these issues by allowing precise dynamical control of the simulated model at the single site level. This includes the geometry of the array, energy offsets on individual tweezers, and the tunneling matrix element on each bond. Going beyond square Hubbard models will enable microscopic studies of qualitatively different phenomena including flat bands, Dirac points, and quantum spin liquids.

The requirements for observing coherent tunneling between two tweezers are the ability to prepare atoms in the motional ground state and to control the energy offset between the tweezers to better than the tunneling energy, which is normally less than a percent of the total depth. In Ref. [17], a two-site Fermi-Hubbard model was realized by loading a pair of tweezers with atoms from a degenerate Fermi gas, with subsequent work measuring correlations and entanglement in coupled two- and three-site systems [34,35]. These experiments have been limited in expanding to large arrays due to the difficulty of *in situ* imaging of  ${}^6\text{Li}$  in optical tweezers [36]. In this Letter, we combine a tweezer array with a quantum gas microscope to study a programmable eight-site Hubbard chain, an increase in the size of the Hilbert space by over three orders of magnitude.

We implement the Fermi-Hubbard model with two hyperfine spin states of  ${}^6\text{Li}$  loaded in a one-dimensional tweezer array. By loading the ground state of four independent tweezers with high fidelity, we adiabatically transform a low-entropy band insulator into a correlated state by ramping on four additional tunnel-coupled tweezers to change the filling of the system. This scheme is similar to proposed adiabatic preparation that allows for single site control of the ramping procedure [37,38]. Near the end of the ramp, the system is well described by the single-band Hamiltonian

$$\hat{H}_{\text{FH}} = - \sum_{(i,j),\sigma} t_{ij} (\hat{c}_{i\sigma}^\dagger \hat{c}_{j\sigma} + \text{H.c.}) + U \sum_i \hat{n}_{i\uparrow} \hat{n}_{i\downarrow} + \sum_{i,\sigma} \Delta_i \hat{n}_{i\sigma}, \quad (1)$$

where  $\hat{c}_{i\sigma}^\dagger$  is the fermionic creation operator of spin  $\sigma$  at site  $i$ , and  $\hat{n}_{i\sigma}$  is the number operator. Here, the local tunneling matrix element  $t_{ij}$ , energy offset  $\Delta_i$ , and on-site interaction  $U$  can be controlled in real time. By carefully controlling the Hubbard parameters, we prepare low entropy states with antiferromagnetic correlations, showcasing the ability of the tweezer platform to generate “clean” many-body systems.

We generate the tweezer array with 770 nm light using an acousto-optical modulator (AOM), such that different tweezers are generated by radio-frequency tones of different frequencies [Fig. 1(a)]. We implement elliptic tweezers with a waist of  $\approx 930$  nm at the atoms as measured along the direction of the tweezer array and a waist of  $\approx 1250$  nm in the perpendicular direction. We work with two different

configurations of the tweezers that we switch between during an experimental cycle: the loading configuration with independent tweezers and the science configuration with tunnel-coupled tweezers at half the separation of the loading configuration. In the science configuration, adjacent tweezers differ in radio-frequency tone by 4 MHz, corresponding to a lattice spacing of 1350 nm. We load the initial configuration of four tweezers from an attractively interacting degenerate gas that is an equal mixture of the lowest and third lowest hyperfine ground states of  ${}^6\text{Li}$  prepared in an optical dipole trap. The initial temperature of the gas is  $\approx 0.2$  times the Fermi temperature, which does not limit the final entropy of the tweezer array [39]. After allowing the system to equilibrate, the optical dipole trap is slowly turned off and the magnetic field is ramped to a noninteracting value.

Initially, there are tens of atoms of each spin state occupying the lowest energy levels of each trap. To remove atoms in higher energy levels, we apply a magnetic gradient while lowering the depth of each trap to spill out all atoms except for one atom in each spin state in the ground state, a technique pioneered in Ref. [39]. Accounting for imaging fidelity, each spin state is loaded with a fidelity  $\langle n_\uparrow \rangle = \langle n_\downarrow \rangle = 0.975(9)$  [40]. We bias the spilling procedure such that almost all of the errors in preparation result in one atom per tweezer and we avoid preparing any atoms in excited motional states. After spilling, we quickly ramp on the additional tweezers needed for the science configuration to  $\sim 95\%$  of the depth of the loading tweezers, corresponding to an energy offset  $\Delta_0$  in Fig. 1(b). In the last stage of the experimental sequence, we slowly decrease the tweezer energy offsets to zero in 50 ms as the scattering

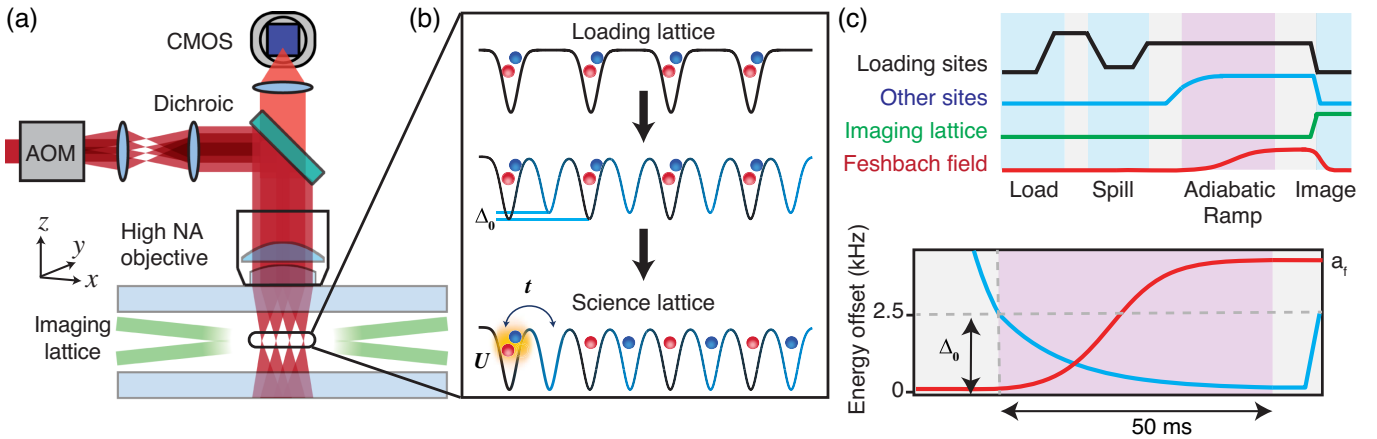


FIG. 1. Experimental setup. (a) The tweezer array is generated by an AOM and is projected through an objective. Correlated states of the Hubbard model are prepared in the array and the atoms are subsequently loaded from the tweezers into a two-dimensional optical lattice in the  $x$ - $y$  plane for imaging [22]. Light scattered during Raman cooling in the 2D lattice is captured through the same objective. (b) Experimental protocol. First, we load the ground state of well-separated tweezers with two atoms in different spin states using a spilling procedure with a magnetic gradient. Next, additional tweezers ramp on to an energy offset  $\Delta_0$  where there is no tunneling. Finally, the energy offset between neighboring tweezers is reduced to zero to adiabatically prepare an antiferromagnetic state. (c) Experimental sequence. To initialize the Fermi-Hubbard array, the energy offset is decreased to zero while the scattering length is increased to its final value  $a_f$ , reaching the desired  $U/t$ .

length of the atoms is ramped to its final value by increasing the magnetic field [see Figs. 1(b) and 1(c)]. Before imaging the resulting correlated state, tunneling is frozen in the array by offsetting the tweezers back to  $\Delta_0$  in 100  $\mu\text{s}$  and increasing the overall depth by a factor of 3. We use the PYTHON package QuSpin to simulate the ramping procedure for comparison to the experiment [41].

Because of its light mass, lithium is a challenging species to image in optical tweezers. Therefore, to detect the atoms with single-site resolution, we transfer them from the tweezer array into a two-dimensional square optical lattice. The lattice has a 752 nm spacing, which allows us to superresolve the array. At a depth of 2500  $E_R$ , the lattice has much larger radial trapping frequencies than the tweezers, which allows us to reach the Lamb-Dicke regime for effective Raman sideband cooling during fluorescence imaging [22]. Using this scheme, we detect atoms with 98.5(4)% fidelity.

For typical tunneling energies of  $h \times 200$  Hz and tweezer depths of  $h \times 50$  kHz, where  $h$  is Planck's constant, we need to balance the intensities of the tweezers to better than 0.5% of the depth to be in the regime where disorder is comparable to or less than the tunneling. This requirement is more stringent than for experiments with Rydberg atoms, which typically only need to equalize the tweezer depths to within a few percent [2,15]. We start by coarsely balancing tweezer intensities on a camera. Fine balancing of tweezer depths in the science configuration is achieved by feeding back on the average density profile of the atoms at  $U/t \sim 1$ , typically taking  $\sim 500$  experimental cycles [40].

In the offset-balanced science configuration array, the atoms realize the Fermi-Hubbard model with disorder less than the tunneling. As the loading fidelity of the band insulator in the loading configuration is not perfect, the system is on average slightly below half filling. After the ramp to the science configuration, the highest  $\langle n \rangle \equiv p$  is 0.955(7), indicating some atom loss during the ramp.

To verify that we can prepare correlated states in the science configuration, we look for Mott insulators at large repulsive interactions, where it is energetically favorable for atoms to be on singly occupied sites. To image singly occupied sites, we first convert atoms on doubly occupied tweezers into Feshbach molecules to ensure loss before loading into the optical lattice [40]. We measure the fraction of singly occupied sites in the Mott insulator as a function of interaction energy (Fig. 2). For this measurement,  $t/h = 160(4)$  Hz, and the scattering length is tuned from 0 to 1600 bohr radii ( $a_0$ ). At a scattering length of  $1600a_0$ , we measure  $U/h = 1.07(4)$  kHz, giving a maximum  $U/t$  of 6.7(3). Using exact diagonalization methods, we extract the expected singles occupation for different densities, and find that the singles occupation we measure at different interactions is consistent with the density  $\langle n \rangle = 0.93(2)$  of this dataset.

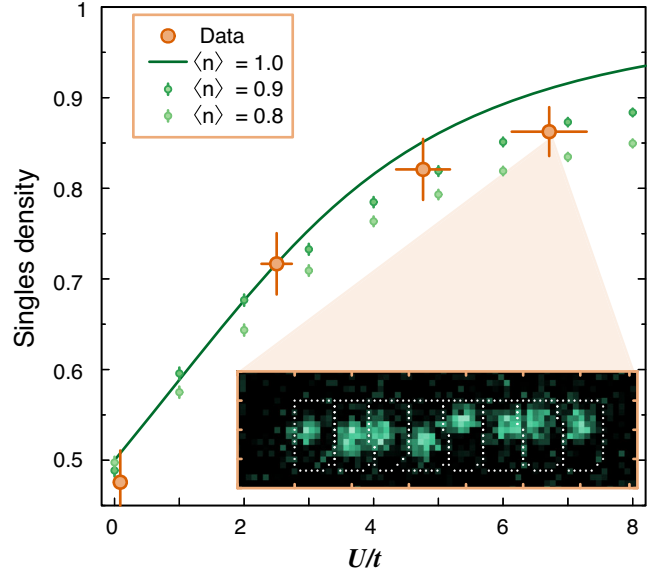


FIG. 2. Singles density as a function of  $U/t$ . We compare the experimental data to the calculated singles density at three different total densities. The measured singles density  $\langle n \rangle = 0.93(2)$  of this dataset is caused by imperfect loading. The inset is a fluorescence image of an eight atom Mott insulator with reconstruction masks (shown as white dotted lines) to identify which tweezer the atom originated from.

Although the suppression of doublons conclusively demonstrates the formation of a correlated state, measurements of the density alone are insufficient to characterize the system at low temperatures. At these temperatures, the atoms preferentially arrange themselves in an antiferromagnetic configuration because of the superexchange interaction. By removing atoms in one spin state with resonant light and imaging the other state (the lowest hyperfine state,  $|\uparrow\rangle$ ), we measure up-up density correlations between sites  $i$  and  $j$  as  $C_{ij} = 4(\langle n_{i\uparrow}n_{j\uparrow} \rangle - \langle n_{i\uparrow} \rangle \langle n_{j\uparrow} \rangle)$  at the largest  $U/t = 6.7(3)$  (Fig. 3). Because of the strong quantum fluctuations, spin correlations in the one-dimensional Fermi-Hubbard model decay over a few sites even in the ground state. For analysis of the correlations, we post-select on imaging four  $|\uparrow\rangle$  atoms, which lowers the effective temperature and increases the filling [40]. We simulate the system using the grand canonical ensemble, defined by chemical potential  $\mu$  and temperature  $T$ , as the atom number in our experiment fluctuates due to imperfect loading [42]. Using a least squares fit on the average atom number and each individual spin correlation, we find a local minimum of temperature at  $k_B T = 0.21(3)t$ , where the error bar is extracted using bootstrapping methods. However, many of the correlators do not have a strong dependence on temperature, and some are non-monotonic with temperature [40]. Around 10% of bootstrapped samples fit to a temperature much closer to zero than the rest of the samples. These temperatures are even lower than the temperature expected from numerically

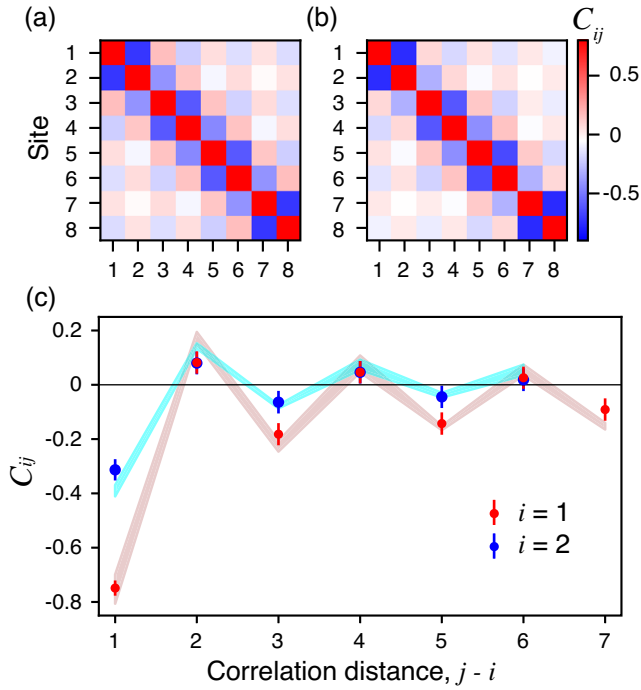


FIG. 3. Antiferromagnetic correlations in the tweezer array. (a) Up-up antiferromagnetic correlations between all lattice sites calculated with exact diagonalization at a temperature  $k_B T = 0.21(3)t$  and (b) experimentally measured correlations for  $U/t = 6.7(3)$ . Because of finite size effects, the edge-nearest neighbor pairs have stronger correlations than other nearest-neighbor pairs. (c) Correlations as a function of distance for the first site (red) and second site (blue) of the chain, corresponding to the first and second rows in the top plots. The shaded curve is the range of calculated correlation values for a specific pair of sites given by the fitted temperature range.

evolving the initial loading configuration. This suggests that spin correlations cease to be a good thermometer at the lowest temperatures we achieve and the fitted temperature is an upper bound.

A more natural quantity to discuss when characterizing closed cold atom systems is the entropy. In the loading configuration, after postselecting on detecting four spin up atoms, the initial entropy is  $0.09(1)k_B$  per particle, calculated from

$$\frac{S}{\langle N \rangle} = -\frac{k_B}{1+p} [p \log p + (1-p) \log(1-p)]. \quad (2)$$

To extract the final entropy after the ramp, we compute the entropy from the fitted grand canonical parameters, obtaining an upper bound on the entropy per particle of  $0.26(4)k_B$ . This entropy is comparable to the lowest entropies measured in optical lattices with fermionic quantum gas microscopes [29–31]. To understand where the entropy gain in the system is coming from, we simulate the ramping procedure and find an expected final entropy of  $0.18(2)k_B$  per particle, which is a lower bound on the

entropy of the system [40]. The dominant source of entropy gain stems from imperfect initial states with a single localized hole, which is an energetically excited state that cannot adiabatically evolve into the ground state of the homogeneous eight-site system. By implementing full spin and density readout in future experiments [43], the entropy of the initial state can be eliminated via postselection. In that case, numerics indicate that nonadiabaticity during the ramp would limit the entropy to  $0.04k_B$  per particle.

Not only can the tweezer platform prepare highly correlated low-entropy equilibrium states, but it can also realize dynamics that are difficult to study in comparable optical lattice systems. To demonstrate the flexibility of the platform, we perform experiments where we prepare atoms only on an edge site of the science configuration and observe the propagation of the particles in the array [Fig. 4(a)]. To initialize dynamics, we decrease the offset from  $\Delta_0$  to zero in  $100 \mu\text{s}$ . In a noninteracting system this experiment is a direct measurement of the tunneling of the array. By comparing our measurements to exact calculations of the tunneling dynamics, we conclude that the tweezers are balanced to within half a tunneling energy.

One other advantage of the tweezer array platform is the ability to easily realize arbitrary lattice geometries. In our one-dimensional system, we explore this by creating a lattice with staggered tunneling. To accomplish this, the radio-frequency tone difference between every other tweezer is changed to 4.2 MHz, with the edge pairs having a spacing of 4 MHz. This leads to a science configuration

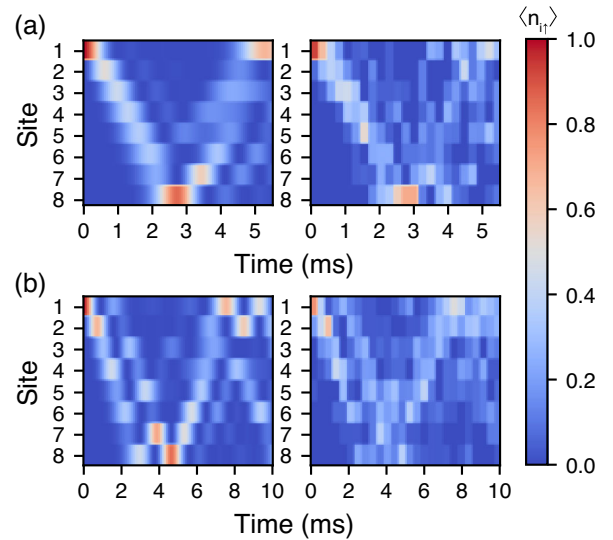


FIG. 4. Pair of noninteracting atoms initialized on one edge site tunneling across the array. (a) Exact diagonalization (left) and experimental (right) dynamics in a configuration with equal tunnelings across all sites. We extract a tunneling rate of  $296(3)$  Hz using a least squares fit. (b) Exact diagonalization (left) and experimental (right) dynamics with staggered tunneling rates. For site  $i$  and site  $j = i + 1$ ,  $t_{ij} = 289(3)$  Hz for odd  $i$  and  $t_{ij} = 213(2)$  Hz for even  $i$ .

where the tunneling is modulated on alternate bonds and hence, qualitatively different behavior than the uniform tunneling array. We study tunneling dynamics in this staggered lattice by initializing atoms on the edge site [Fig. 4(b)]. There is good qualitative agreement with simulations, with two ballistically propagating tunneling trajectories forming before the atoms reach the opposite side of the chain. However, since dynamical experiments are intrinsically more sensitive to disorder than studying ground states, deviations of the data from the simulations are more significant.

In conclusion, we have shown that optical tweezer arrays can be used to prepare many-body states of lattice fermions. The key advantages over optical lattices are increased flexibility in engineering Hubbard models on arbitrary geometry lattices and, with full postselection on the atom number and spin, the possibility of reaching very low entropy states limited only by adiabaticity of the preparation. This platform is particularly well suited to studying ground states of many-body systems at high  $U/t$  and at half-filling, where residual disorder plays a negligible role. It is feasible to extend our system to arrays of up to a hundred tweezers as has been demonstrated by the Rydberg atom array community [4,5], especially since the tweezer balancing algorithm runtime is approximately independent of the number of tweezers. To scale the tweezer array to two dimensions, we plan to use two crossed acousto-optic deflectors, with the second dimension introduced by stroboscopically switching between chains created using the approach described in this Letter. This will allow studying 2D Hubbard models with arbitrary software-defined geometry and microscopic measurements of correlations in phases yet to be explored with quantum gas microscopes, including quantum spin liquids in triangular or hexagonal geometries and flat-band ferromagnets in Lieb lattices.

We would like to thank Lysander Christakis, Lawrence Cheuk, and Max Prichard for helpful discussions. This work was supported by the NSF (Grant No. 2110475), the David and Lucile Packard Foundation (Grant No. 2016-65128), and the ONR (Grant No. N00014-21-1-2646).

\*Present address: Department of Physics, Harvard University, Cambridge, Massachusetts 02138, USA.

†Corresponding author.  
wbakr@princeton.edu

- [1] D. Barredo, S. De Léséleuc, V. Lienhard, T. Lahaye, and A. Browaeys, *Science* **354**, 1021 (2016).
- [2] M. Endres, H. Bernien, A. Keesling, H. Levine, E. R. Anschuetz, A. Krajenbrink, C. Senko, V. Vuletić, M. Greiner, and M. D. Lukin, *Science* **354**, 1024 (2016).
- [3] A. M. Kaufman and K.-K. Ni, *Nat. Phys.* **17**, 1324 (2021).
- [4] P. Scholl, M. Schuler, H. J. Williams, A. A. Eberharter, D. Barredo, K.-N. Schymik, V. Lienhard, L.-P. Henry, T. C. Lang, T. Lahaye, A. M. Läuchli, and A. Browaeys, *Nature (London)* **595**, 233 (2021).
- [5] S. Ebadi, T. T. Wang, H. Levine, A. Keesling, G. Semeghini, A. Omran, D. Bluvstein, R. Samajdar, H. Pichler, W. W. Ho, S. Choi, S. Sachdev, M. Greiner, V. Vuletić, and M. D. Lukin, *Nature (London)* **595**, 227 (2021).
- [6] A. Cooper, J. P. Covey, I. S. Madjarov, S. G. Porsev, M. S. Safronova, and M. Endres, *Phys. Rev. X* **8**, 041055 (2018).
- [7] M. A. Norcia, A. W. Young, and A. M. Kaufman, *Phys. Rev. X* **8**, 041054 (2018).
- [8] S. Saskin, J. T. Wilson, B. Grinkemeyer, and J. D. Thompson, *Phys. Rev. Lett.* **122**, 143002 (2019).
- [9] L. Liu, J. Hood, Y. Yu, J. Zhang, N. Hutzler, T. Rosenband, and K.-K. Ni, *Science* **360**, 900 (2018).
- [10] L. Anderegg, L. W. Cheuk, Y. Bao, S. Burchesky, W. Ketterle, K.-K. Ni, and J. M. Doyle, *Science* **365**, 1156 (2019).
- [11] H. Labuhn, D. Barredo, S. Ravets, S. De Léséleuc, T. Macrì, T. Lahaye, and A. Browaeys, *Nature (London)* **534**, 667 (2016).
- [12] H. Bernien, S. Schwartz, A. Keesling, H. Levine, A. Omran, H. Pichler, S. Choi, A. S. Zibrov, M. Endres, M. Greiner, V. Vuletić, and M. D. Lukin, *Nature (London)* **551**, 579 (2017).
- [13] H. Levine, A. Keesling, G. Semeghini, A. Omran, T. T. Wang, S. Ebadi, H. Bernien, M. Greiner, V. Vuletić, H. Pichler, and M. D. Lukin, *Phys. Rev. Lett.* **123**, 170503 (2019).
- [14] I. S. Madjarov, J. P. Covey, A. L. Shaw, J. Choi, A. Kale, A. Cooper, H. Pichler, V. Schkolnik, J. R. Williams, and M. Endres, *Nat. Phys.* **16**, 857 (2020).
- [15] A. W. Young, W. J. Eckner, W. R. Milner, D. Kedar, M. A. Norcia, E. Oelker, N. Schine, J. Ye, and A. M. Kaufman, *Nature (London)* **588**, 408 (2020).
- [16] A. Kaufman, B. Lester, C. Reynolds, M. Wall, M. Foss-Feig, K. Hazzard, A. Rey, and C. Regal, *Science* **345**, 306 (2014).
- [17] S. Murmann, A. Bergschneider, V. M. Klinkhamer, G. Zürn, T. Lompe, and S. Jochim, *Phys. Rev. Lett.* **114**, 080402 (2015).
- [18] I. Bloch, *Nat. Phys.* **1**, 23 (2005).
- [19] L. Tarruell and L. Sanchez-Palencia, *C.R. Phys.* **19**, 365 (2018).
- [20] D. Greif, M. F. Parsons, A. Mazurenko, C. S. Chiu, S. Blatt, F. Huber, G. Ji, and M. Greiner, *Science* **351**, 953 (2016).
- [21] L. W. Cheuk, M. A. Nichols, K. R. Lawrence, M. Okan, H. Zhang, and M. W. Zwierlein, *Phys. Rev. Lett.* **116**, 235301 (2016).
- [22] P. T. Brown, D. Mitra, E. Guardado-Sanchez, P. Schauß, S. S. Kondov, E. Khatami, T. Paiva, N. Trivedi, D. A. Huse, and W. S. Bakr, *Science* **357**, 1385 (2017).
- [23] L. W. Cheuk, M. A. Nichols, K. R. Lawrence, M. Okan, H. Zhang, E. Khatami, N. Trivedi, T. Paiva, M. Rigol, and M. W. Zwierlein, *Science* **353**, 1260 (2016).
- [24] M. F. Parsons, A. Mazurenko, C. S. Chiu, G. Ji, D. Greif, and M. Greiner, *Science* **353**, 1253 (2016).
- [25] M. Boll, T. A. Hilker, G. Salomon, A. Omran, J. Nespolo, L. Pollet, I. Bloch, and C. Gross, *Science* **353**, 1257 (2016).
- [26] J. Vijayan, P. Sompert, G. Salomon, J. Koepsell, S. Hirthe, A. Bohrdt, F. Grusdt, I. Bloch, and C. Gross, *Science* **367**, 186 (2020).
- [27] G. Ji, M. Xu, L. H. Kendrick, C. S. Chiu, J. C. Brüggenjürgen, D. Greif, A. Bohrdt, F. Grusdt, E. Demler, M. Lebrat, and M. Greiner, *Phys. Rev. X* **11**, 021022 (2021).

- [28] J. Koepsell, J. Vijayan, P. Sompet, F. Grusdt, T. A. Hilker, E. Demler, G. Salomon, I. Bloch, and C. Gross, *Nature (London)* **572**, 358 (2019).
- [29] A. Mazurenko, C. S. Chiu, G. Ji, M. F. Parsons, M. Kanász-Nagy, R. Schmidt, F. Grusdt, E. Demler, D. Greif, and M. Greiner, *Nature (London)* **545**, 462 (2017).
- [30] P. T. Brown, D. Mitra, E. Guardado-Sanchez, R. Nourafkan, A. Reymbaut, C.-D. Hébert, S. Bergeron, A.-M. Tremblay, J. Kokalj, P. Schauß, and W. S. Bakr, *Science* **363**, 379 (2019).
- [31] P. Sompet, S. Hirthe, D. Bourgund, T. Chalopin, J. Bibo, J. Koepsell, P. Bojović, R. Verresen, F. Pollmann, G. Salomon, C. Gross, T. Hilker, and I. Bloch, *arXiv:2103.10421*.
- [32] P. A. Lee, N. Nagaosa, and X.-G. Wen, *Rev. Mod. Phys.* **78**, 17 (2006).
- [33] C. S. Chiu, G. Ji, A. Mazurenko, D. Greif, and M. Greiner, *Phys. Rev. Lett.* **120**, 243201 (2018).
- [34] A. Bergschneider, V. M. Klinkhamer, J. H. Becher, R. Klemt, L. Palm, G. Zürn, S. Jochim, and P. M. Preiss, *Nat. Phys.* **15**, 640 (2019).
- [35] J. H. Becher, E. Sindici, R. Klemt, S. Jochim, A. J. Daley, and P. M. Preiss, *Phys. Rev. Lett.* **125**, 180402 (2020).
- [36] A. Bergschneider, V. M. Klinkhamer, J. H. Becher, R. Klemt, G. Zürn, P. M. Preiss, and S. Jochim, *Phys. Rev. A* **97**, 063613 (2018).
- [37] M. Lubasch, V. Murg, U. Schneider, J. I. Cirac, and M.-C. Bañuls, *Phys. Rev. Lett.* **107**, 165301 (2011).
- [38] M. R. Sturm, M. Schlosser, R. Walser, and G. Birkel, *Phys. Rev. A* **95**, 063625 (2017).
- [39] F. Serwane, G. Zürn, T. Lompe, T. Ottenstein, A. Wenz, and S. Jochim, *Science* **332**, 336 (2011).
- [40] See Supplemental Material at <http://link.aps.org/supplemental/10.1103/PhysRevLett.128.223202> for further experimental details and entropy calculations.
- [41] P. Weinberg and M. Bukov, *SciPost. Phys.* **7**, 020 (2019).
- [42] A. M. Kaufman, M. E. Tai, A. Lukin, M. Rispoli, R. Schittko, P. M. Preiss, and M. Greiner, *Science* **353**, 794 (2016).
- [43] J. Koepsell, S. Hirthe, D. Bourgund, P. Sompet, J. Vijayan, G. Salomon, C. Gross, and I. Bloch, *Phys. Rev. Lett.* **125**, 010403 (2020).